Applied Materials Today 20 (2020) 100623

Contents lists available at ScienceDirect

Applied Materials Today

journal homepage: www.elsevier.com/locate/apmt

Stretchable electromagnetic fibers for self-powered mechanical sensing

Zhuolin Du[a,1], Jingwei Ai[b,1], Xuan Zhang[a,d], Zheng Ma[a], Zhenhua Wu[a], Dezhi Chen[b], Guangming Tao[c], Bin Su[a,*]

[a] State Key Laboratory of Material Processing and Die & Mould Technology, School of Materials Science and Engineering, Huazhong University of Science and Technology, Wuhan 430074, Hubei, PR China
[b] State Key Laboratory of Advanced Electromagnetic Engineering and Technology, School of Electrical and Electronic Engineering, Huazhong University of Science and Technology, Wuhan 430074, Hubei, PR China
[c] Wuhan National Laboratory for Optoelectronics, School of Optical and Electronic Information, Huazhong University of Science and Technology, Wuhan 430074, Hubei, PR China
[d] ARC Hub for Computational Particle Technology, Department of Chemical Engineering, Monash University, Clayton, VIC 3800, Australia

ARTICLE INFO

Article history:
Received 17 December 2019
Received in revised form 5 March 2020
Accepted 10 March 2020

Keywords:
Electromagnetic
Fibers
Self-powered
Mechanical sensing

ABSTRACT

Fiber based sensors may enable a new class of wearable electronics due to their high flexibility, great breathability and direct integration into daily clothes, but progress is hindered by the power supply model that greatly restricts their duration and user experiences. Here we report the fabrication of stretchable electromagnetic fibers that can recognize mechanical forces with a self-powered feature. Conductive wires were twined outside stretchable magnetic fibers, enabling relative movements between magnetic and conductive fibers during cycles of stretching/recovery. Therefore, those electromagnetic fibers can sense the applied forces based on electromagnetic induction effect. Tuning fabrication parameters, such as magnetic powder content, fiber diameter and the number of twined conductive wires, can improve the performance of electromagnetic fibers. Owing to self-powered sensing capacity, flexibility and long-term durability, such electromagnetic fibers were attached onto fiver fingers of a robotic hand to endow the robot with a self-perception capacity. Our study employs a scalable wet-spinning method to prepare electromagnetic fibers and illustrates the critical design concept to obtain optimized electromagnetic performances of those fibers, which would facilitate further development of fibertronics and wearable electronics.

1. Introduction

Fiber sensors are a branch of fibertronics [1], and has received growing attention due to their bendable/twistable capacities, feasible textile processability and long working lifetime [2]. Generally, fiber sensors detect the human motions based on the change of resistance [3], capacity [4], voltage [5] or optical density [6,7] caused by their physical deformation, and are ideal candidates for real-time monitoring of human bodies. Compared with film-based electronic skins (e-skins), knitted fibers result in loose air pores over the fabric, allowing human skins to breathe easier [8]. As a result, the users feel comfortable and tend to wear the fiber sensors in daily lives. Another advantage of fiber sensors is their easy & invisible integration to the human clothing because of their inherent fiber nature [9]. Therefore, tremendous efforts have been paid in this field to exploit diverse fiber-based sensing devices [10,11].

Early fiber sensors are driven by external power supply, such as portable lithium batteries, indicating limited running life and inconvenience to recharge/replace the batteries [12]. Alternatively, self-powered concepts, by using photovoltaic [13–15], thermoelectric [16–18], piezoelectric [19–21] or triboelectric [22–24] mechanisms, have been proposed in recent decades for maintaining the sensor working without the batteries. Photovoltaic fibers can obtain power from the sunshine, however, might be prevented in rainy days or indoor environment. Thermoelectric fibers are excellent to convert thermo to electric energy. Notably, brittleness, high-cost fabrication as well as unsatisfactory permeability of the fabrics prevent their practical in textile sensors [25]. Piezoelectric or triboelectric fibers can convert mechanical to electric energy rapidly, but their considerable internal impedances (>10^5 Ω) are an open question that might raise inherent loss of the power supply itself [26,27].

Electromagnetic induction effect, found by Michael Faraday in 1831 [28,29], is another avenue to convert mechanical to electri-

* Corresponding author.
E-mail address: subin@hust.edu.cn (B. Su).
[1] These authors contributed equally to this work.

https://doi.org/10.1016/j.apmt.2020.100623
2352-9407/

cal energy. An interesting attempt was reported by Donelan et al. [30] that they invented an electromagnetic device attaching to the human legs. Walking with such a device can generate electricity >5 Watts. However, the whole device consisted of rigid gear trains and magnets, indicating heavy and uncomfortable user experiences. Furthermore, several groups [31–35] demonstrated the possibility to convert biomechanical to electric energy by either directly fixing a rigid magnet on the clothing [31] or placing the rigid magnets in the hollow spheres [32,33] or tubes [34,35]. Relative movements between the magnets and the coils can generate electricity when the people are running, walking or shaking. However, the heavy & rigid magnets upon the clothing make them neither beautiful nor practical. It is expected that lightweight & flexible magnetic fibers can circumvent this challenge [25], and show promising self-powered feature in wearable electronics.

In this study, we report the preparation of stretchable electromagnetic fibers to overcome the above challenge. NdFeB magnetic powders, up to 70 wt%, were introduced and stably dispersed in the elastic Ecoflex scaffold to fabricate stretchable (strain >50%) & magnetic (>40 mT) fibers through a wet-spinning method. A conductive wire was twined outside each magnetic fiber, allowing relative movements between magnetic and conductive fibers during one cycle of stretching/recovery. Owing to such material/structural designs, mechanically stretching/bending forces can be sensed and recognized with a self-powered feature due to the electromagnetic induction effect. Several fabrication parameters, such as magnetic powder content, fiber diameter and the number of twined conductive wires, have been tuned to improve the performance of electromagnetic fibers. We also demonstrate the stable electric robustness after 5000 stretching-recovery cycles. Finally, such self-powered electromagnetic fibers were attached onto fiver fingers of a robotic hand to endow the robot with a self-perception capacity. Our electromagnetic fibers offer a general tactic toward self-powered fiber sensors for the development of other wearable energy converting devices.

2. Results and discussion

Fig. 1a shows the preparation process of stretchable electromagnetic fibers through a wet-spinning method. Wet-spinning is a scalable fiber production technology that has been widely used in industrial fields [36]. Owing to its versatile & continuous production features, wet-spinning method has been used in this study. At first, the wet-spinning composite formulation was prepared by dispersing NdFeB magnetic powders (diameter of $26 \pm 6\,\mu m$, see Supplemental Figure S1) in the viscous Ecoflex liquid without magnetization. After being stirred for more than one hour, the black & homogeneous formulation liquid was ejected into an ethanol bath, resulting in long continuous fibers after a heating process. The diameter of the fibers was controlled to be ~2 mm, which was comparable to that of Zn–air fiber-shaped batteries [37] or super-stretchable electroluminescent fibers [38]. To obtain a uniformly oriented magnetic field in the fibers, a magnetizing post-treatment was conducted treating the North pole perpendicular to the fibers. Then, a conductive wire was twined with each magnetic fiber

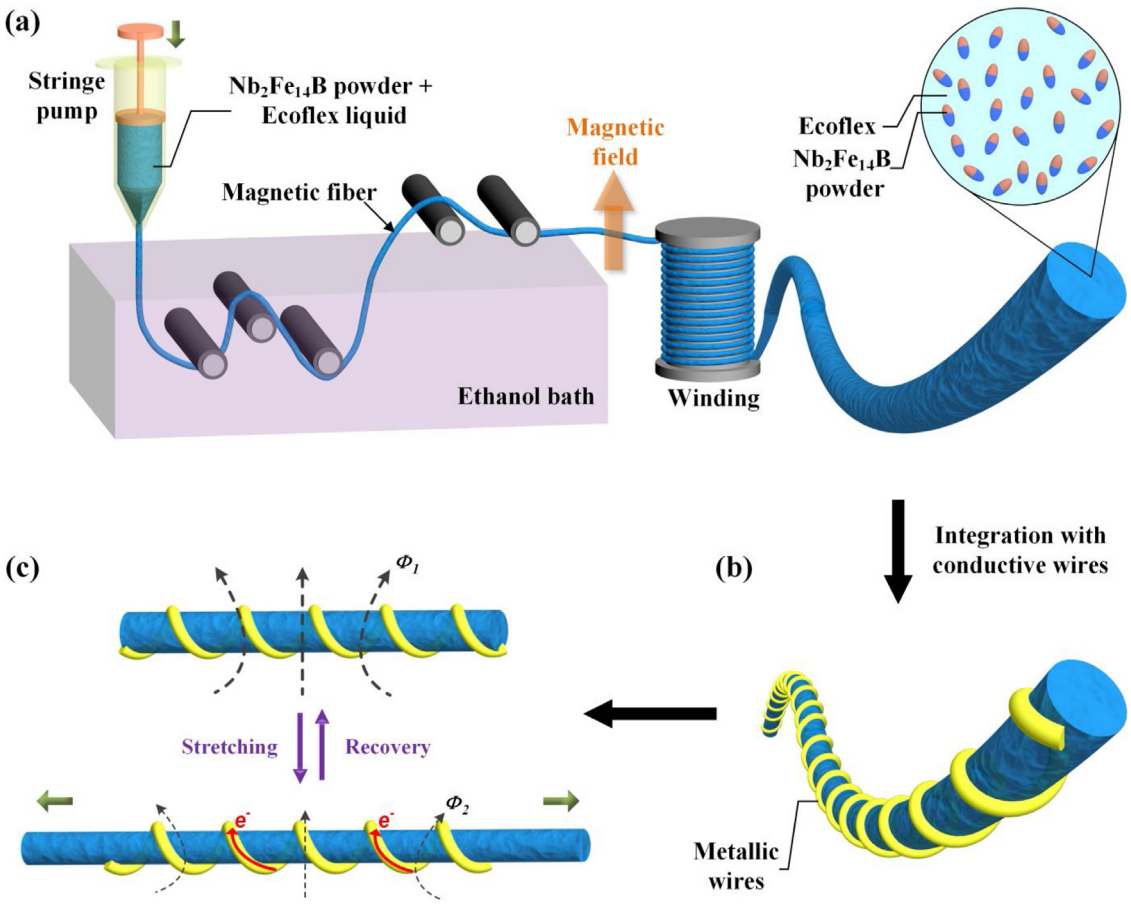

Fig. 1. Schematic illustration of the preparation process for stretchable electromagnetic fibers through a wet-spinning technique. (a) A black & homogeneous formulation liquid consisting of NdFeB magnetic powders and Ecoflex liquid was ejected into an ethanol bath, resulting in long continuous fibers after a heating process. To obtain a uniformly oriented magnetic field in the fibers, a magnetizing post-treatment was conducted treating the North pole perpendicular to the fibers. (b) A conductive wire was twined with the magnetic fiber, resulting in stretchable electromagnetic fibers. (c) Relative movements between magnetic and conductive fibers during cycles of stretching/recovery enable electromagnetic fibers to recognize mechanical forces with a self-powered feature.

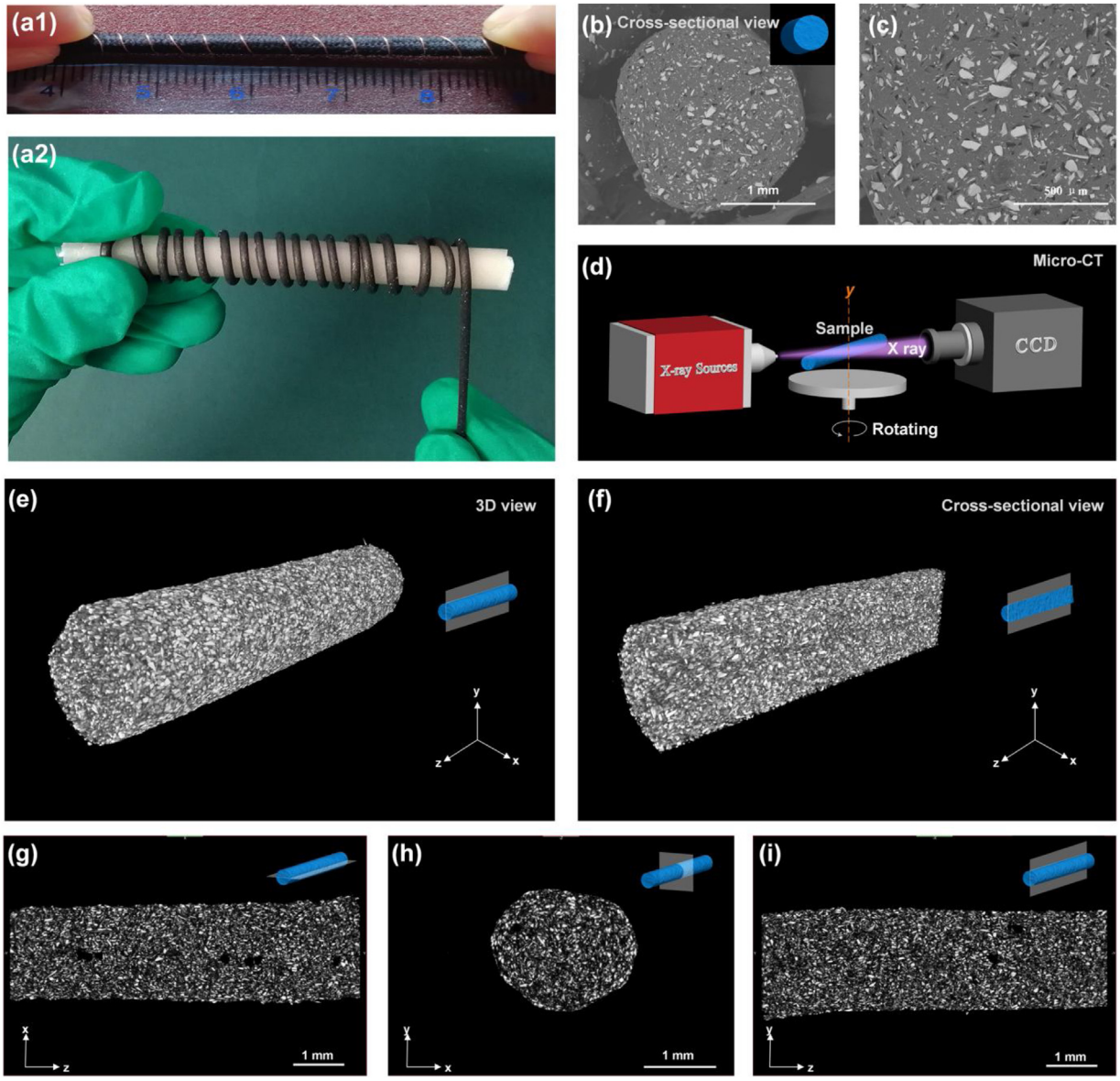

Fig. 2. Structural characterizations of stretchable electromagnetic fibers. Optical images of (a1) one electromagnetic fiber that is composed of (a2) one 70 wt% NdFeB magnetic fiber twisted by a conductive copper wire. The magnetic fiber part can twine upon a rod, indicating its flexibility. (b) Cross-sectional scanning electron microscope (SEM) view of the magnetic fiber. (c) Is magnified image of (b). (d) Schematic illustration of the sample tested in the micro computerized tomography (micro-CT) system. 3D reconstructed images of a (e) full and (f) half magnetic fiber. Sliced micro-CT images of the magnetic fiber in (g) *x*-*z*, (h) *x*-*y* and (i) *y*-*z* planes.

(Fig. 1b). Spiral structures of the conductive wires allow them to deform/recover when being stretched. In this case, stretchable electromagnetic fibers consisting of straight magnetic fibers and spiral conductive wires were fabricated, entitled as HUST-5.

The structural observations of stretchable NdFeB/Ecoflex (70/30 wt%) magnetic fibers were conducted. Fig. 2a shows the optical photograph of one as-prepared electromagnetic fiber. Continuous black fibers can twine upon a plastic rod, exhibiting their well mechanical flexibility. Furthermore, the cross-section of one magnetic fiber was investigated by scanning electron microscope (SEM) photos (Fig. 2b,c). Bright and dark regions represent the magnetic powders and silicone elastomer, respectively. It is clearly observed that NdFeB magnetic powders were uniformly dispersed in the Ecoflex host material. Besides two-dimensional (2D) SEM images, we also employed micro computerized tomography (micro CT) system to obtain three-dimensional (3D) distribution of NdFeB magnetic powders inside the fibers (Fig. 2d). Micro-CT technology is a non-invasive, in-site method to obtain full structural analysis of composites, and has been applied in many research areas [39]. Fig. 2e,f are 3D reconstructed graphs of one magnetic fiber while Fig. 2g–i are their sliced images in *x*-*z*, *x*-*y*, and *y*-*z* planes, respectively. Bright and gray (a little light than dark) regions represent the magnetic powders and silicone elastomer due to their different absorption of X-ray. Both micro-CT and SEM results show that the magnetic powders were homogeneously dispersed no matter upon or inside the NdFeB/Ecoflex composite fibers.

Since the dispersion of magnetic powders was uniform, the magnetic intensities in different positions along the fibers were similar, around 40 ± 4 mT (Supplemental Figure S2). Moreover, such a magnetic intensity remained after being stored in the room temperature for more than one week, indicating the long-term stability of magnetic fibers. Owing to highly elastic Ecoflex scaffolds, the magnetic fibers were easy to stretch (Supplemental Figure S3a). Their stress-strain lines can be found in Supplemental Figure S3b. It is observed that the stretch curve lies above the recovery curve, resulting in a hysteresis loop after the finish of stretching pro-

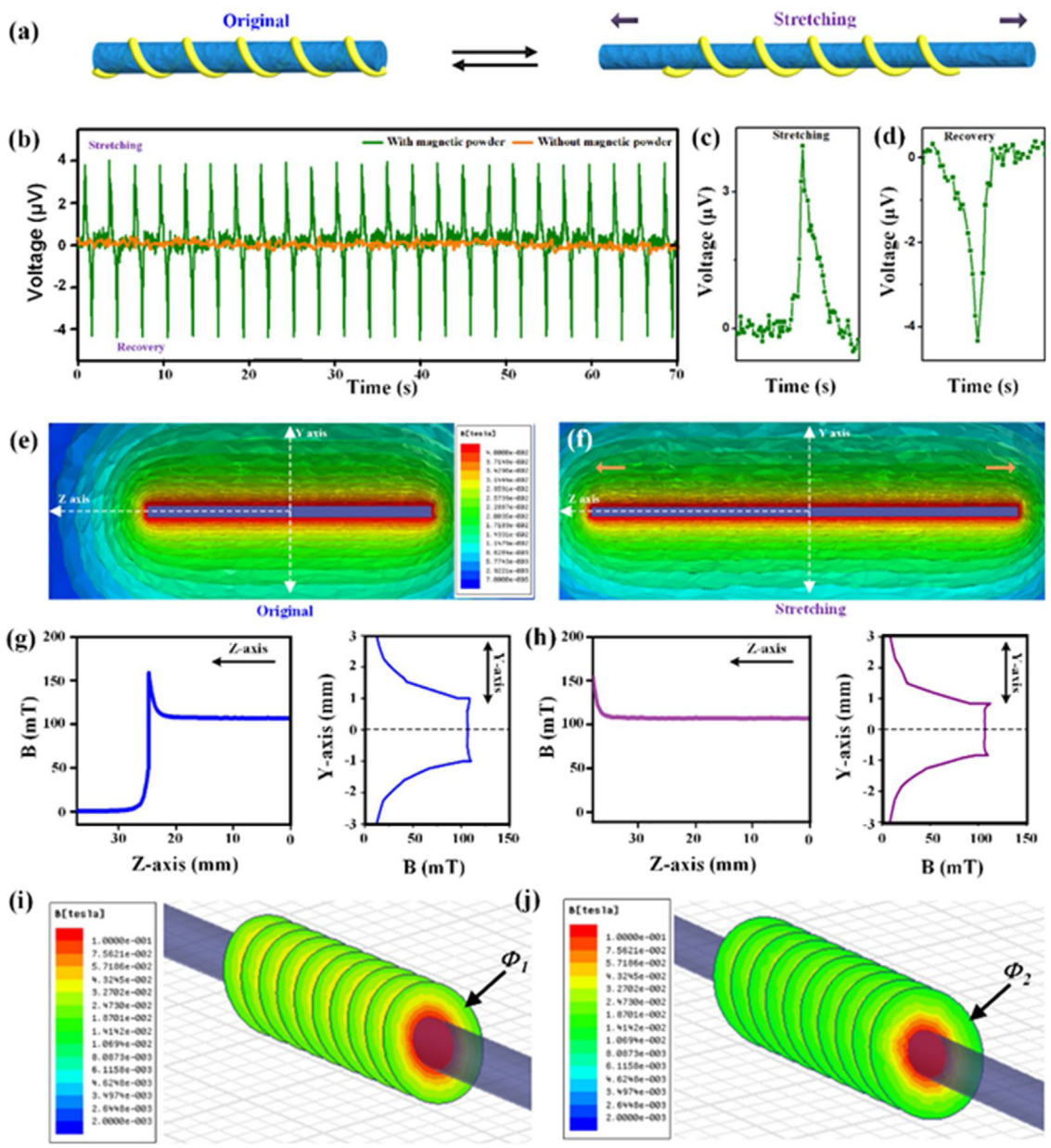

Fig. 3. Self-powered sensing of stretchable electromagnetic fibers. (a) Schematic diagram of one electromagnetic fiber before/after stretching. (b) The open-circuit time-output voltage curve of one electromagnetic fiber by stretching at a speed of 50 mm s^{-1} and a strain of 50% at room temperature. (c, d) The magnified output voltage curves during one cycle of stretching/recovery process. 3D calculated magnetic intensity distributions of the fiber sample at the (e) before and (f) after being stretched. The curves of the magnetic intensity along the *Z*-axis and *Y*-axis (g) before and (h) after being stretched. The 3D calculated magnetic intensity distributions of twined coils (i) before and (j) after being stretched.

Table 1
Calculated and measured voltages of electromagnetic fibers before/after stretching.

The diameter of the tested fiber (mm)	Φ_1 (Wb × 10^{-6})	Φ_2 (Wb × 10^{-6})	$\Delta\Phi$ (Wb × 10^{-6})	Δt (s)	Calculated voltage (μV)	Measured voltage (μV)
2	1.49	1.05	−0.44	0.11	3.9	3.8

cess [40]. The magnetic fibers remained well after being stretched, which has been proved by the micro-CT images shown in Supplemental Figure S4. The magnetic fiber shows a reduced diameter when being stretched with a strain of ~50%. Notably, even after undergoing more than 1000 times stretching-recovery cycles, no crack or fracture could be found upon/inside the fiber, exhibiting well tensile properties of as-prepared magnetic fibers.

Owing to permanent magnetism, stability and stretchability, a NdFeB/Ecoflex (70/30 wt%) magnetic fiber with a length of 50 mm and a diameter of 2 mm was twined by a conductive wire, then tested its electromagnetic performance (Fig. 3a). In our design, one magnetic fiber led to a local magnetic field around, yielding stable magnetic flux passing through each conductive coil twined upon the fiber. External stretching force caused the physical deformation, as well as the magnetic intensity distribution, of the fiber. Therefore, the magnetic flux passing through each conductive coil would change, resulting in the electrical generation. To verify this design concept, we fixed one electromagnetic fiber on a translation

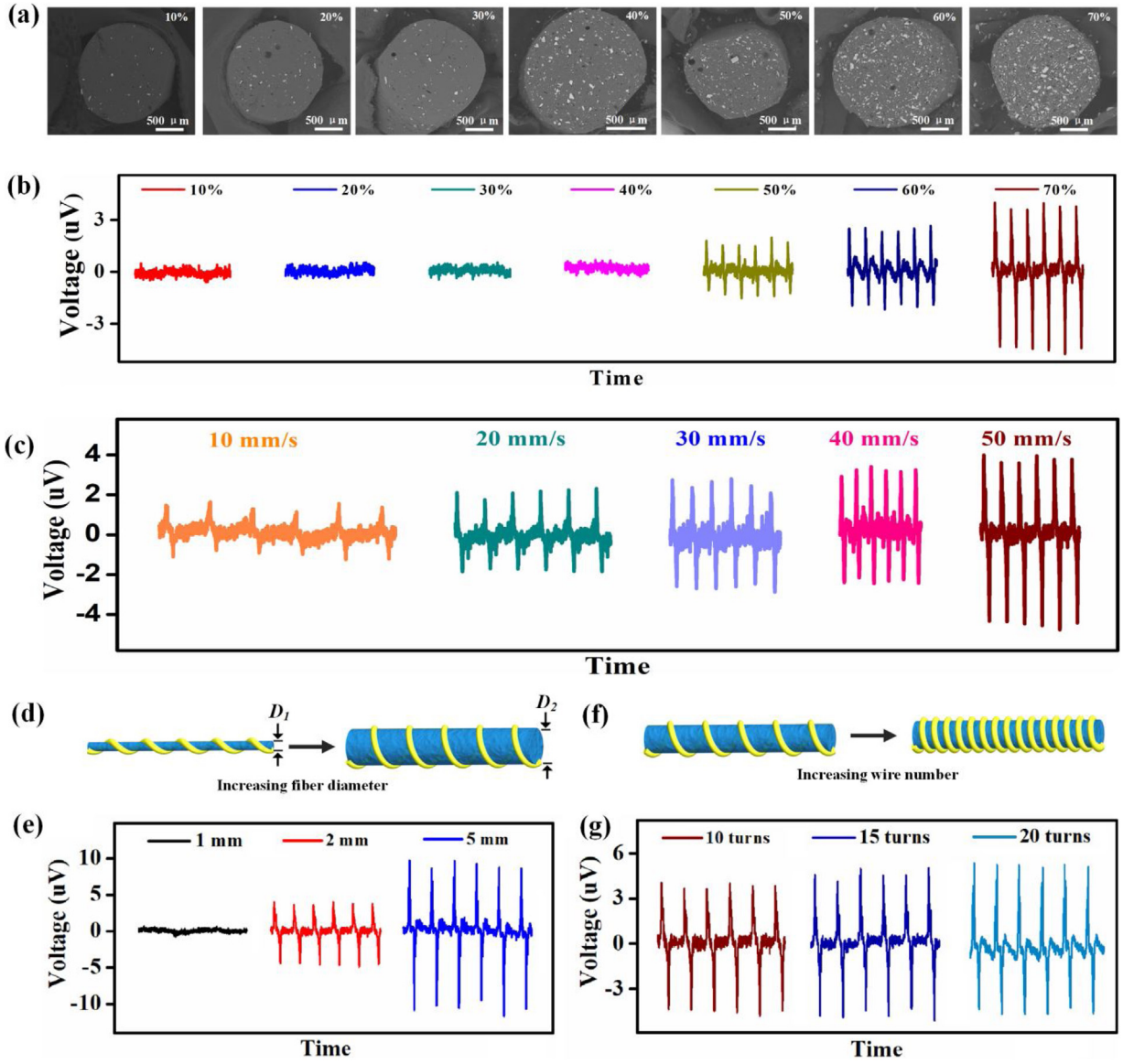

Fig. 4. Different parameters that can affect the performance of stretchable electromagnetic fibers. (a) Cross-sectional SEM images of magnetic fibers with the magnetic powder contents from 10 wt% to 70 wt%. (b) According output voltage-time curves of those magnetic fibers. (c) Output voltage-time curves of electromagnetic fibers testing by applying differnt stretching speeds. Schematic diagrams of electromagnetic fibers fabricated with (d) dfferent numbers of conductive coils and (f) diverse diameters of magnetic fibers. (e) and (g) are output voltage-time curves of (d) and (f), respectively. In above-mentioned experiments, only one parameter was changed while other conditions remained unless indicated otherwise.

stage which can provide controllable stretching force. Then, a continuous curve with regular output voltage peaks and valleys can be found when being stretched with a 50% strain at a speed of 50 mm/s, shown in Fig. 3b. Magnified curves of one stretching/recovery cycle were exhibited in Fig. 3c and Fig. 3d, respectively. The upward peak (stretching process) and downward peak (recovery process) of 3.8 ± 0.1 μV were clearly observed.

The working mechanism of electromagnetic fibers can be explained with the assistance of Ansys Maxwell numerical simulation. The NdFeB/Ecoflex (70/30 wt%) magnetic fiber can be simplified as an unary magnetic system (Fig. 3e,i). The simulation modeling employed a 2D static magnetic field solver with horizontal Z-axis and vertical *X*-axis. The unary magnetic system was set as a fiber 2 mm (*diameter*) × 5 mm (length), followed by magnetizing in the direction of positive *Y*-axis. The color bar, from blue to red, represents gradually increased magnetic intensity. It clearly shows that the strongest magnetic intensity appears along the fiber. The twined conductive wires were equivalent to the same number of concentric rings with a tilting angle of 30 degree. As a result, the total magnetic flux of the electromagnetic fiber before/after stretching can be calculated by below Eq. (1) [40–42]:

$$E(V) = -N \cdot \frac{\Delta \Phi}{\Delta t} = -\sum_{i=1}^{i} \frac{\Delta \Phi_i}{\Delta t} = -\sum_{i=1}^{i} \frac{\Phi_i(after) - \Phi_i(before)}{\Delta t} \quad (1)$$

where $E(V)$ is output voltage, N is the number of concentric rings of the tilted wire, $\Delta\Phi$ is total magnetic flux change, $\Delta\Phi_i$ is magnetic flux change of each equivalent ring, Δt is the response time of the fiber.

When being applied a stretching strain, the electromagnetic fiber would be thinner, inducing a reduced magnetic flux passing through the rings (Fig. 3f,j). The magnetic intensity distributions of the fiber along the *Z* and *Y* axes before/after stretching can be found in Fig. 3g and h, respectively. The stretching of fiber led to decreased magnetic intensity along the *Y*-axis. The total magnetic flux changes through the rings before/after stretching can

be calculated according to Eq. (1). Taking the 50% strain as an example, the total magnetic flux through the copper rings before and after the stretching is 1.49×10^{-6} Wb and 1.05×10^{-6} Wb (see Table 1), respectively. As a result, the change of magnetic flux is -0.44×10^{-6} Wb. The stretching time of the fiber is 112 ms, yielding a theoretically calculated voltage value of 3.9 μV, which fits the experimental result of 3.8 μV in average (Fig. 3b) well. Experimental and theoretical differences of output voltage values mainly attributed to the practical/ideal distributions of conductive rings. During the stretching/recovery processes, the rings would be slightly close/separated, yielding a tight difference from the ideal state in the simulation model.

We then investigated the electromagnetic performance of as-prepared fibers by tuning different fabrication and testing parameters. According to Eq. (1), the magnetic intensity (B), stretching time (Δt) and the number of coils (N) can affect the final voltage output. Thus, we tailored the magnetic intensity (B) by decreasing the content of NdFeB magnetic powers in the fibers from 70 wt% to 10 wt%, and according cross-sectional SEM images can be found in Fig. 4a. Clearly, the amount of magnetic particles in the fibers becomes denser following the increase of their mass ratio. The magnetic field intensities and Young modulus of such a series of magnetic fibers can be found in Supplemental Figure S5. When the mass ratio of magnetic powders was enhanced from 10 wt% to 70 wt%, according magnetic field intensity of the fibers increased from only 2 mT to around 40 mT while the Young modulus of fibers rose from 2.09 MPa to 5.71 MPa. Lower magnetic field intensity indicates smaller change of magnetic flux through the coils, yielding a tiny voltage output. As shown in Fig. 4b, 70 wt% electromagnetic fiber delivered the highest output voltage (Fig. 4b). In the meanwhile, the peaks and valleys of the curves with the mass ratio below 50 wt% could hardly be found.

Stretching time (Δt) was decided by the testing speed of the translation stage. Therefore, Fig. 4c exhibits the influence of stretching speed on the electromagnetic performance of fibers with a 70 wt% magnetic content. Higher speed indicated shorter stretching time, leading to higher voltage output. The fiber showed an output voltage of 3.8 μV at a stretching speed of 50 mm/s while that of 1.4 μV at a stretching speed of 10 mm/s. On the other hand, the strain of fibers did not show obvious influence on the electromagnetic performance of fibers (Supplemental Figure S6). During the strain of 25% and 50%, the electrical outputs were similar to each other. This result might attribute to tiny change of magnetic field during such strains. In contrast, increasing the number of coils twined on the magnetic fibers can increase the output voltage (Fig. 4d,e). The fiber showed enhanced output voltages from 3.8 μV to 5.9 μV by doubling the coil number. Enlarging the fiber diameter could effectively increase the magentic intensity around the fiber (Supplemental Figure S7), as well as favor the output voltage (Fig. 4f,g). When the diameter of the fiber was tuned from 2 mm to 5 mm, the voltage increased significantly from 3.8 μV up to 9.1 μV. Thinner fibers, such as a diameter of 1 mm, yielded lower voltage.

The cycling stability of electromagnetic fibers was tested, shown in Fig. 5. The sample with a 70 wt% magnetic content and a diameter of 2 mm was fixed on the translation stage with 5000 stretching/recovery circles at a strain of 50% and speed of 50 mm/s. Even after thousands of physical deformations then recovery, the fiber could still maintain a stable output voltage without obvious hysteresis or attenuation. Implying that as-prepared electromagnetic fibers owned a long-term working stability.

Since the electromagnetic fibers can provide a self-powered sensing ability to external force, we demonstrate that they can be used to assist the self-perception of robots. Different from human beings, robots cannot feel the external forces without the tactile

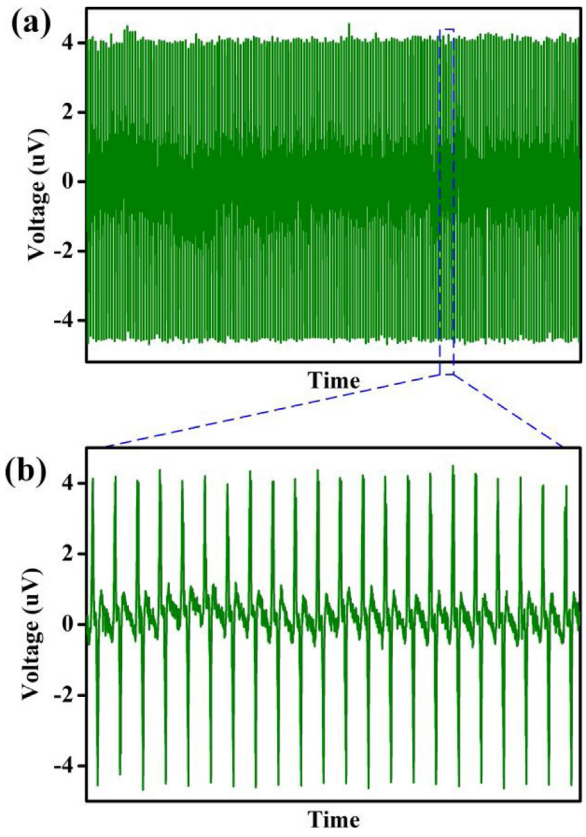

Fig. 5. Long-term performance stability of stretchable electromagnetic fibers. (a) Output voltage-time curve and (b) magnified graph of the electromagnetic fiber with 5000 stretching/recovery circles at a strain of 50% and speed of 50 mm/s. (a) Is sliced part from 4000–5000 cycles.

sensors. However, additional sensors would increase the weight of robots, as well as the extra power consuming. Our electromagnetic fibers were flexible, lightweight and could sense external forces without additional power supply. Thus, we fixed five electromagnetic fibers onto five fingers of a robotic hand (Fig. 6a). The ends of fibers were anchored on the bendable fingers by closely sealed tapes (Fig. 6b), allowing the fiber to deform following the motion of fingers. The home positions of five fingers can be found in Fig. 6d. When the hand posed from "one" to "five" as different gestures, the fibers would exhibit diverse voltage signals (Fig. 6c). Taking the gesture "one" as an example, the fore finger was bent backwards, leading to the compression of the fiber attached on it. Thus, the voltage was negative. In contrast, fibers attached to the thumb, little finger, ring finger and middle finger were bent forwards, yielding the stretching of fibers and positive voltage peaks (Fig. 6c). Thus, forward/backward direction information of the input signals can be distinguished accordingly. Similar to gesture "one", different hand motions yielded diverse finger movements, which can be recognized by different positive/negative voltage signals. By analyzing such electrical results, the robot hand can own the self-perception capacity for further adaptive motions [9,43,44].

Generally, electromagnetic fibers generated larger current while triboelectric or piezoelectric counterparts yielded higher voltage. These differences enable them to adapt to different application requirements. To prove this concept, we measured the current output of electromagnetic fibers and compared with reported results by triboelectric or piezoelectric fibers (Fig. 7). The open-circuit time-current curve of one electromagnetic fiber with a 70 wt% magnetic content at a stretching speed of 50 mm s^{-1} and a strain of 50% at room temperature can be found in Fig. 7a. The upward

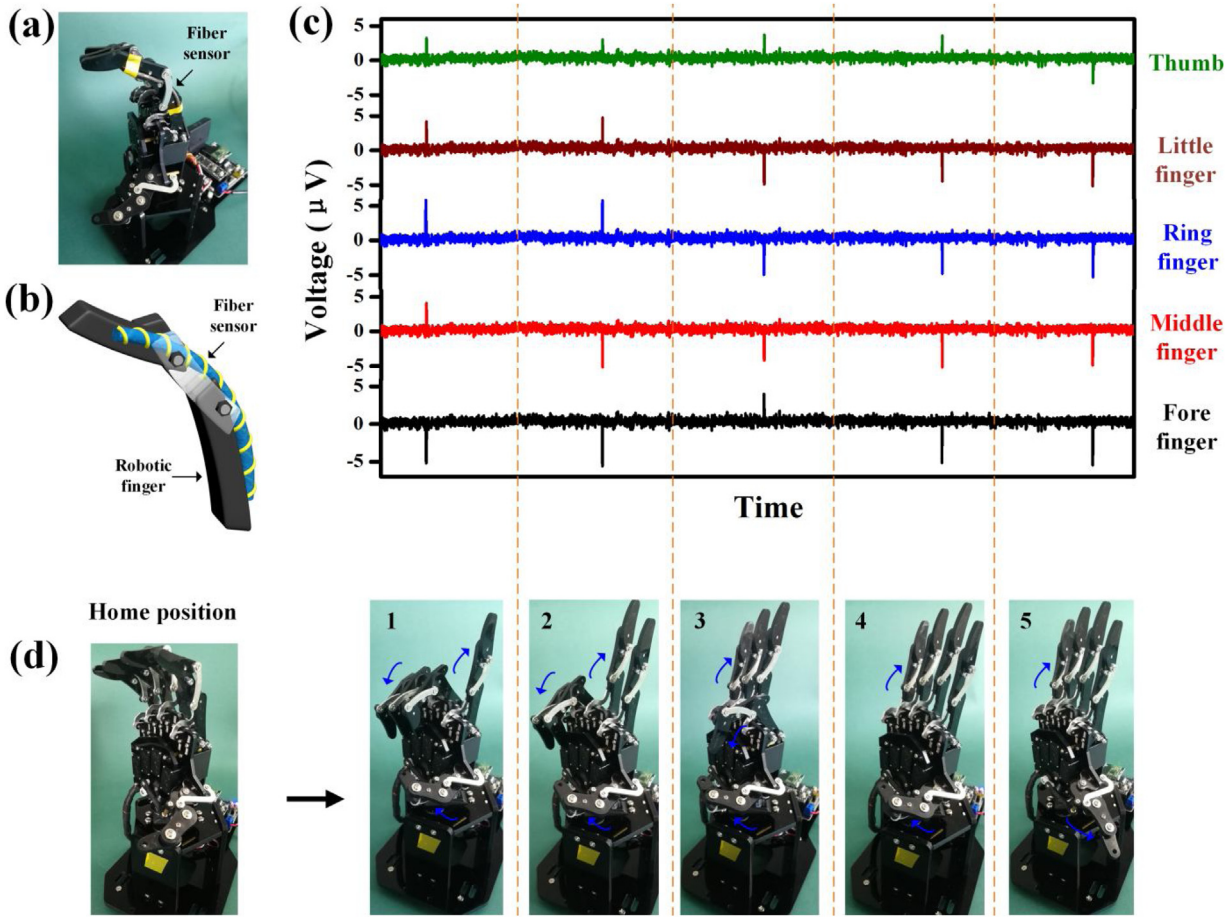

Fig. 6. Self-perception capacity for a robotic hand by using stretchable electromagnetic fibers. (a) Photograph of a robotic hand with five free moving fingers controlled by a program. (b) Schematic illustration shows that each finger was attached by an electromagnetic fiber. (c) Output voltage-time curves of electromagnetic fibers upon those five fingers when the hand posed from "one" to "five" as different gestures. (d) Photographs of the robotic hand in home position and those by posing different gestures.

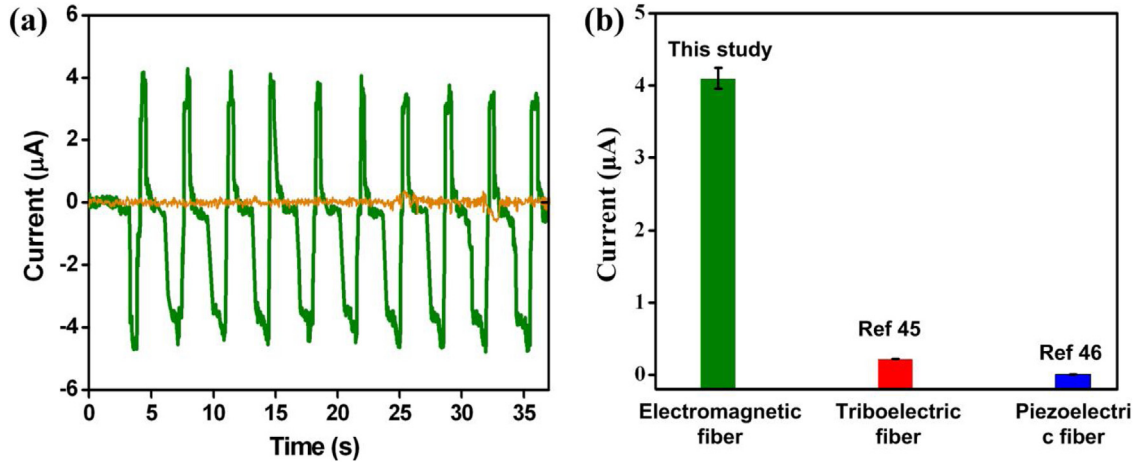

Fig. 7. Current outputs of stretchable electromagnetic fibers. (a) The open-circuit time-output current curve of one electromagnetic fiber by stretching at a speed of 50 mm s^{-1} and a strain of 50% at room temperature. (b) Accroding histogram of output current comparison among electromagnetic, triboelectric and piezoelectric fibers.

peak (stretching process) and downward peak (recovery process) of 3.9 ± 0.2 μA were clearly observed. In contrast, reported current outputs by triboelectric [45] or piezoelectric [46] fibers are only tens of nanoamperometers (Fig. 7b), which are a few magnitude lower than that of electromagnetic fibers. Therefore, different strategies have different advantages. The electromagnetic fibers have relatively higher output current while triboelectric or piezoelectric fibers created higher output voltage.

3. Conclusion

We demonstrate the fabrication of stretchable electromagnetic fibers that can sense the external force in a self-powered model. Mechanical forces can be converted to electrical energy for maintaining the working of electromagnetic fibers, indicating their low-cost running feature. As-prepared electromagnetic fibers showed well stretchability (strain up to 50%), long-term magnetic

& electrical robustness and tunable electromagnetic performances. Though the output voltage for a single fiber was not high (up to 9.1 μV), the electrical performance is reasonably believed to improve by increasing the numbers of fibers or coils. This study is just the beginning of electromagnetic fibers. Further studies are expected to construct complex fiber arrays that might favor the development of wearable electronics.

Authors' contributions

Bin Su conceived the idea and designed the sensor. Zhuolin Du, Xuan Zhang, Zheng Ma, Zhenhua Wu fabricated the sensor and performed the experiments. Jingwei Ai did the numerical simulation. Zhuolin Du, Dezhi Chen, Guangming Tao and Bin Su analyzed the data and prepared the manuscript. All authors discussed the results and commented on the manuscript.

Declaration of Competing Interest

The authors declare that they have no known competing financial interests or personal relationships that could have appeared to influence the work reported in this paper.

Acknowledgements

This work was supported by International Postdoctoral Exchange Fellowship Program (Talent-Introduction Program), the National 1000 Young Talents Program of China and initiatory financial support from HUST. The authors also thank the technical supports from Huazhong University of Science and Technology Analytical & Testing Center.

Appendix A. Supplementary data

Supplementary material related to this article can be found, in the online version, at https://doi.org/10.1016/j.apmt.2020.100623.

References

[1] D.R. Seshadri, R.T. Li, J.E. Voos, J.R. Rowbottom, C.M. Alfes, C.A. Zorman, C.K. Drummond, NPJ Digit. Med. 2 (2019) 71.
[2] N. Wiegand, M. Haupt, E. Mäder, C. Cherif, Adv. Eng. Mater. 18 (2016) 385–390.
[3] P. Li, L. Zhao, Z. Jiang, M. Yu, Z. Li, X. Zhou, Y. Zhao,Sci. Rep. 9 (2019), 14457.
[4] X. Zhang, W. Lu, G. Zhou, Q. Li, Adv. Mater. (2019) 1902028.
[5] X. Wang, Y. Zhang, X. Zhang, Z. Huo, X. Li, M. Que, Z. Peng, H. Wang, C. Pan, Adv. Mater. 30 (2018) 1706738.
[6] S. Kwon, Y.H. Hwang, M. Nam, H. Chae, H.S. Lee, Y. Jeon, S. Lee, C.Y. Kim, S. Choi, E.G. Jeong, K.C. Choi, Adv. Mater. (2019) 1903488.
[7] Y. Liang, Z. Yu, L. Li, T. Xu,Sci. Rep. 9 (2019), 7379.
[8] W. Weng, P. Chen, S. He, X. Sun, H. Peng, Angew. Chem. Int. Ed. 55 (2016) 6140–6169.
[9] Y. Mengüç, Y.-L. Park, H. Pei, D. Vogt, P.M. Aubin, E. Winchell, L. Fluke, L. Stirling, R.J. Wood, C.J. Walsh, Int. J. Robot. Res. 33 (2014) 1748–1764.
[10] X. He, Y. Zi, H. Guo, H. Zheng, Y. Xi, C. Wu, J. Wang, W. Zhang, C. Lu, Z.L. Wang, Adv. Funct. Mater. 27 (2017) 1604378.
[11] H.M. Kim, J.H. Park, S.K. Lee,Sci. Rep. 9 (2019), 15605.
[12] X. Pu, W. Hu, Z.L. Wang, Small 14 (2018) 1702817.
[13] H. Li, Z. Yang, L. Qiu, X. Fang, H. Sun, P. Chen, S. Pan, H. Peng, J. Mater. Chem. A 2 (2014) 3841–3846.
[14] H. Sun, X. You, J. Deng, X. Chen, Z. Yang, J. Ren, H. Peng, Adv. Mater. 26 (2014) 2868–2873.
[15] Z. Zhang, Z. Yang, J. Deng, Y. Zhang, G. Guan, H. Peng, Small 11 (2015) 675–680.
[16] A.R.M. Siddique, S. Mahmud, B.V. Heyst, Renew. Sustain. Energy Rev. 73 (2017) 730–744.
[17] L. Zhang, S. Lin, T. Hua, B. Huang, S. Liu, X. Tao, Adv. Energy Mater. 8 (2018) 1700524.
[18] G. Zuo, O. Andersson, H. Abdalla, M. Kemerink, Appl. Phys. Lett. 112 (2018) 083303.
[19] A. Almusallam, Z. Luo, A. Komolafe, K. Yang, A. Robinson, R. Torah, S. Beeby, Nano Energy 33 (2017) 146–156.
[20] B. Li, F. Zhang, S. Guan, J. Zheng, C. Xu, J. Mater. Chem. C 4 (2016) 6988–6995.
[21] Y. Qin, X. Wang, Z.L. Wang, Nature 451 (7180) (2008) 809–813.
[22] K. Dong, J. Deng, W. Ding, A.C. Wang, P. Wang, C. Cheng, Y.-C. Wang, L. Jin, B. Gu, B. Sun, Z.L. Wang, Adv. Energy Mater. 8 (2018) 1801114.
[23] K. Dong, Z. Wu, J. Deng, A.C. Wang, H. Zou, C. Chen, D. Hu, B. Gu, B. Sun, Z.L. Wang, Adv. Mater. 30 (2018) 1804944.
[24] R. Hinchet, H.-J. Yoon, H. Ryu, M.-K. Kim, E.-K. Choi, D.-S. Kim, S.-W. Kim, Science 365 (2019) 491–494.
[25] J. Shi, S. Liu, L. Zhang, B. Yang, L. Shu, Y. Yang, M. Ren, Y. Wang, J. Chen, W. Chen, Y. Chai, X. Tao, Adv. Mater. (2019) 1901958.
[26] F. Narita, M. Fox, Adv. Eng. Mater. 20 (2018) 1700743.
[27] K.S. Ramadan, D. Sameoto, S. Evoy, Smart Mater. Struct. 23 (2014) 033001.
[28] T.N. Do, H. Phan, T.-Q. Nguyen, Y. Visell, Adv. Funct. Mater. 28 (2018) 1800244.
[29] L.C. Rome, L. Flynn, E.M. Goldman, T.D. Yoo, Science 309 (2005) 1725–1728.
[30] J.M. Donelan, Q. Li, V. Naing, J.A. Hoffer, D.J. Weber, A.D. Kuo, Science 319 (2008) 807–810.
[31] H. Lee, J.-S. Roh, Text. Res. J. 89 (2018) 2532–2541.
[32] Z. Lin, B. Zhang, H. Guo, Z. Wu, H. Zou, J. Yang, Z.L. Wang, Nano Energy 64 (2019) 103908.
[33] Y. Rao, S. Cheng, D.P. Arnold, J. Micromech. Microeng. 23 (2013) 114012.
[34] H. Liu, Z. Ji, T. Chen, L. Sun, S.C. Menon, C. Lee, IEEE Sens. J. 15 (2015) 4782–4790.
[35] Q. Zhang, Y. Wang, E.S. Kim, J. Appl. Phys. 115 (2014) 064908.
[36] S. Ling, D.L. Kaplan, M.J. Buehler, Nat. Rev. Mater. 3 (2018) 18016.
[37] Y. Xu, Y. Zhang, Z. Guo, J. Ren, Y. Wang, H. Peng, Angew. Chem. -Int. Ed. 54 (2015) 15390–15394.
[38] Z. Zhang, L. Cui, X. Shi, X. Tian, D. Wang, C. Gu, E. Chen, X. Cheng, Y. Xu, Y. Hu, J. Zhang, L. Zhou, H.H. Fong, P. Ma, G. Jiang, X. Sun, B. Zhang, H. Peng, Adv. Mater. 30 (2018) 1800323.
[39] L. Sumner-Rooney, N.J. Kenny, F. Ahmed, S.T. Williams,Sci. Rep. 9 (2019), 15411.
[40] X. Zhang, J. Ai, Z. Ma, Z. Du, D. Chen, R. Zou, B. Su, J. Mater. Chem. C 7 (2019) 8527–8536.
[41] Z. Wu, J. Ai, Z. Ma, X. Zhang, Z. Du, Z. Liu, D. Chen, B. Su, ACS Appl. Mater. Int. 11 (2019) 44865.
[42] X. Zhang, J. Ai, Z. Ma, Z. Du, D. Chen, R. Zou, B. Su, Nano Energy 69 (2020) 104391.
[43] J. Ge, X. Wang, M. Drack, O. Volkov, M. Liang, G.S. Canon Bermudez, R. Illing, C. Wang, S. Zhou, J. Fassbender, M. Kaltenbrunner, D. Makarov,Nat. Commun. 10 (2019), 4405.
[44] J. Park, M. Kim, Y. Lee, H.S. Lee, H. Ko,Sci. Adv. 1 (2015), e1500661.
[45] T.M. Zhao, J.L. Li, H. Zeng, Y.M. Fu, H.X. He, L.L. Xing, Y. Zhang, X.Y. Xue, Nanotechnology 29 (2018) 405504.
[46] X. Lu, H. Qu, M. Skorobogatiy, ACS Nano 11 (2017) 2103.